Acta Crystallographica Section A
Foundations of Crystallography
ISSN 0108-7673

Received 4 June 2008
Accepted 29 August 2008

Extending the S-FFT direct-methods algorithm to density functions with positive and negative peaks. XIV

Jordi Rius* and Carles Frontera

Institut de Ciència de Materials de Barcelona (CSIC), Campus de la UAB, 08193-Bellaterra, Catalunya, Spain. Correspondence e-mail: jordi.rius@icmab.es

Some years ago the direct-methods origin-free modulus sum function (S) was adapted to the processing of intensity data from density functions with positive and negative peaks [Rius, Miravitlles & Allmann (1996). *Acta Cryst*. A**52**, 634–639]. That implementation used phase relationships explicitly. Although successfully applied to different situations where the number of reflections was small, its generalization to larger problems required avoiding the time-consuming manipulation of quartet terms. To circumvent this limitation, a modification of the recently introduced S-FFT algorithm (that maximizes S with only Fourier transforms) is presented here. The resulting S_2-FFT algorithm is highly effective for crystal structures with at least one moderate scatterer in the unit cell. Test calculations have been performed on conventional single-crystal X-ray diffraction data, on neutron diffraction data of compounds with negative scatterers and on intensities of superstructure reflections to solve difference structures.

1. Introduction

The solution of the phase problem of X-ray crystallography by direct methods, *i.e.* from the measured intensities and the existing relationships between their associated phases φ, can be formulated as a constrained global minimization problem. Two important constrained phase-refinement functions are (i) the cosine minimal function (Debaerdemaeker & Woolfson, 1983; DeTitta *et al.*, 1994)

$$R_{\rm C}(\Phi) = \Big(\sum_{\mathbf{h}}\sum_{\mathbf{k}} A_{\mathbf{hk}}\Big)^{-1} \sum_{\mathbf{h}}\sum_{\mathbf{k}} A_{\mathbf{hk}}\big[\cos(\varphi_{-\mathbf{h}} + \varphi_{\mathbf{k}} + \varphi_{\mathbf{h}-\mathbf{k}}) - I_1(A_{\mathbf{hk}})/I_0(A_{\mathbf{hk}})\big]^2, \quad (1)$$

in which the observed magnitudes are the conditional expected values of the cosine of the triple-phase sums that, for crystal structures belonging to $P1$ and containing N atoms in the unit cell, correspond to the ratio of the modified Bessel functions of the first and zeroth orders with argument $A_{\mathbf{hk}}$ defined by $2N^{-1/2}|E_{-\mathbf{h}}||E_{\mathbf{k}}||E_{\mathbf{h}-\mathbf{k}}|$ (Germain *et al.*, 1970; Cochran, 1955); and (ii) the residual minimizing the squared differences between the observed moduli of the structure factors G and the calculated ones expressed in terms of the collectivity of phases Φ of the strong reflections,

$$R_G(\Phi) = \sum_{\mathbf{H}} \big[|G_{\mathbf{H}}| - |G_{\mathbf{H}}(\Phi)|\big]^2 \Big/ \sigma_{\mathbf{H}}^2, \quad (2)$$

where the errors or discrepancies $|G_{\mathbf{H}}| - |G_{\mathbf{H}}(\Phi)|$ are assumed to be random and distributed according to a Gaussian density function with variances $\sigma_{\mathbf{H}}^2$. The structure factors $G = |G|\exp(i\psi)$ are the Fourier coefficients of the squared density function (corrected for form factor and thermal vibration decay). For a unit cell with N equal scatterers and $P1$ symmetry, $|G|$ is proportional to the normalized structure-factor moduli $|E|$ of the true structure:

$$|G| = (1/N^{1/2})\,|E|. \quad (3)$$

Both phase-refinement functions have their own advantages and limitations. $R_{\rm C}$ was first checked by Debaerdemaeker & Woolfson (1983) with rather poor results. However, when alternated with peak search in real space as in the *SnB* strategy (DeTitta *et al.*, 1994), its ability to refine phases improves dramatically. One important advantage of equation (1) is that it only uses large E values and the triplets among them. This keeps the number of triplets manageable even for relatively large structures and ensures its applicability to situations where no weak E values are available. As a counterpart it considers individual cosine estimates, which become less accurate as the unit-cell contents increase. From a practical point of view, continuous switching between the reciprocal-space part (triplets) and the real-space part (Fourier synthesis) complicates the implementation. One of the principal differences between equations (1) and (2) is the active use of the weak E values that the latter makes. This fact confers on R_G great robustness, so that alternating between reciprocal- and direct-space parts is, in principle, not necessary. If the moduli $|G|$ are calculated with the expression (Rius, 1993)

$$|G_{\mathbf{H}}(\Phi)| = V^{-1} \sum_{\mathbf{h}} |E_{\mathbf{h}}||E_{\mathbf{H-h}}| \exp i(\psi_{-\mathbf{H}} + \varphi_{\mathbf{h}} + \varphi_{\mathbf{H-h}}) \quad (4)$$

and the same variance is assumed for all **H**, minimization of R_G is equivalent to maximizing the origin-free modulus sum function (Rius, 2006)

$$\begin{aligned} S &= \sum_{\mathbf{H}} \big(|G_{\mathbf{H}}| - \langle|G|\rangle\big)|G_{\mathbf{H}}(\Phi)| \\ &= (1/N^{1/2}) \sum_{\mathbf{H}} \big(|E_{\mathbf{H}}| - \langle|E|\rangle\big)|G_{\mathbf{H}}(\Phi)|, \end{aligned} \quad (5)$$

where $\langle|G|\rangle$ and $\langle|E|\rangle$ are the average $|G_{\mathbf{H}}|$ and $|E_{\mathbf{H}}|$ values, respectively. This function has proven very effective for solving crystal structures. The solution is performed by maximizing S in terms of the phases of the large reflections with the origin-free modulus sum function tangent formula S-TF (Rius, 1993):

$$\tan \varphi_{\mathbf{h}} = \frac{\sum_{\mathbf{H}} \big(|E_{\mathbf{H}}| - \langle|E|\rangle\big)|E_{\mathbf{h-H}}| \sin(\psi_{\mathbf{H}} + \varphi_{\mathbf{h-H}})}{\sum_{\mathbf{H}} \big(|E_{\mathbf{H}}| - \langle|E|\rangle\big)|E_{\mathbf{h-H}}| \cos(\psi_{\mathbf{H}} + \varphi_{\mathbf{h-H}})}. \quad (6)$$

In this iterative process the ψ parameters are assumed to be equal to the respective φ parameters for the strong reflections, whereas, for the weak ones, the ψ values are periodically recalculated from the new phase estimates of the large reflections. Unlike the original tangent formula (Karle & Hauptman, 1956), this improved one is not affected by the uranium-atom solution. One inherent limitation of the S function when explicitly expressed as a function of the cosine of the triple-phase sums is the large number of terms involved in its computation. This is a consequence of the inclusion of the weak E values. One way to reduce the number of triplets is to raise the threshold limit value for considering an E value as large in the calculation of $|G|$ from equation (4). However, this is at the cost of the accuracy of $|G|$. The number of cosine terms becomes even larger when the density function can have positive and negative peaks. Since in this case the approximation $\rho \simeq \rho^2$ cannot be used, it is the similarity between ρ and ρ^3 that has to be employed in the definition of the modulus sum function (Rius *et al.*, 1996). This causes the appearance of double summations in the numerator and in the denominator of the corresponding modified tangent formula. This generalized S function was applied to a superstructure of index 2 to demonstrate that direct methods do not require the positivity condition. It has subsequently been used for solving projected reconstructed surface structures from in-plane fractional rods measured by the synchrotron GIXRD technique (Torrelles *et al.*, 1998; Hirnet *et al.*, 2002). However, its application to out-of-plane data is hampered by the large number of phase relationships generated in its computation. Recently, Rius *et al.* (2007) presented a new optimization strategy of the S function that takes advantage of the fast Fourier transform (FFT) algorithm, thus avoiding the explicit calculation of the phase relationships. They introduce the complex quantities

$$D_{\mathbf{H}} = (|E_{\mathbf{H}}| - \langle|E|\rangle) \exp(i\psi_{\mathbf{H}}) \quad (7)$$

as Fourier coefficients of a modified density function called $\rho'_{\rm sq}$. Then, in view of equations (4) and (7), S in equation (5) can be rewritten in the form

$$S = K \sum_{\mathbf{h}} |E_{-\mathbf{h}}| \exp(i\varphi_{-\mathbf{h}}) \Big[V^{-1} \sum_{\mathbf{H}} D_{\mathbf{H}}(\Phi) E_{\mathbf{h-H}} \Big] \quad (8)$$

with K equal to $N^{1/2}$. The sum within the brackets concerns the Fourier coefficients (Q) of the product function $\rho_Q = \rho\rho'_{\rm sq}$. This product can be easily performed in real space, and the Q coefficients are then readily obtained by Fourier inverting ρ_Q. The new phase estimates optimizing S are the phases of Q,

$$\varphi_{\mathbf{h}(\rm new)} = \text{phase of } \big\{Q_{\mathbf{h}}(\Phi_{\rm old})\big\}. \quad (9)$$

2. The S-FFT phase-refinement method in the absence of the equal-sign condition

2.1. The squared-shape density function ρ_2

Experimentally, the structure-factor amplitudes $|G|$ of the squared density distribution (ρ^2) are not directly measurable quantities. However, for crystal structures with N equal scatterers in the unit cell following $P1$ space-group symmetry, $|G|$ can be derived from the observed $|E|$ through the simple relationship (3). However, equation (3) is not valid for structures possessing mixed positive and negative scatterers, since ρ and ρ^2 are no longer proportional. The introduction of the so-called squared-shape density function (ρ_2) allows this difficulty to be circumvented. In this function the peaks have the same shape as they have in ρ^2 but the same signs as they have in ρ. Consequently, the corresponding structure-factor moduli $|G_2|$ are proportional to the observed $|E|$ values and expression (3) still holds:

$$\big|G_2\big| = (1/N^{1/2})\,|E|. \quad (10)$$

Important for the practical application of ρ_2 is the calculation of $|G_2|$ as a function of the Φ phases. This requires the introduction of the mask $m(\mathbf{r})$, defined by

$$m(\mathbf{r}) = \begin{cases} 1 & \text{if } \rho(\mathbf{r}) < t\sigma(\rho) \\ -1 & \text{if } \rho(\mathbf{r}) < -t\sigma(\rho) \\ 0 & \text{if } -t\sigma(\rho) < \rho(\mathbf{r}) < t\sigma(\rho), \end{cases} \quad (11)$$

where $\mathbf{r}$ ranges over the whole unit cell. In general t is taken close to 2.5. The product of ρ^2 with m preserves in the resulting modified density function not only the signs that the peaks have in ρ but also the shapes they have in ρ^2. Consequently the Fourier coefficients of $(\rho^2 m)$ are the desired $G_2(\Phi)$. By writing $m(\mathbf{r})$ as the Fourier series

$$m(\mathbf{r}) = V^{-1} \sum_{\mathbf{K}} |M_{\mathbf{K}}| \exp(i\alpha_{\mathbf{K}}) \exp(-i2\pi \mathbf{Kr}), \quad (12)$$

then by applying the Fourier theory, $G_2(\Phi)$ can be expressed in terms of the coefficients of ρ and m by means of the double summation

$$\begin{aligned} G_{2,-\mathbf{H}}(\Phi) = V^{-2} \sum_{\mathbf{K}} |M_{\mathbf{K}}| \sum_{\mathbf{h}} |E_{-\mathbf{h}}||E_{-\mathbf{H+h-K}}| \\ \times \exp i(\alpha_{\mathbf{K}} + \varphi_{-\mathbf{h}} + \varphi_{-\mathbf{H+h-K}}). \end{aligned} \quad (13)$$

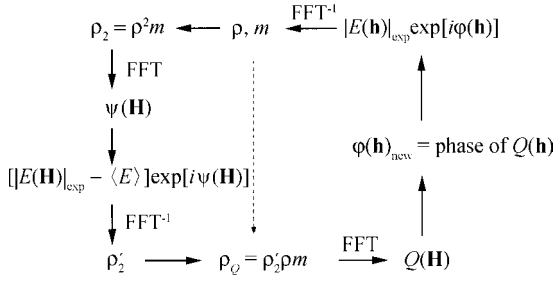

Figure 1
S_2-FFT phase-refinement procedure. The initial phases (upper right corner) are combined with the experimental amplitudes to compute the electron density ρ and the associated mask m. The mask is used to compute the phases ψ of the squared-shape density function and also (broken arrow) the product function ρ_Q. The Fourier transform of ρ_Q yields the new structure-factor estimates.

Notice that the condition that all peaks in ρ have the same sign (equal-sign condition) is not used in the derivation of equation (13).

2.2. The *S* function without equal-sign condition (S_2)

If both moduli $|G_{\mathbf{H}}|$ and $|G_{\mathbf{H}}(\Phi)|$ are replaced in equation (5) by the corresponding $|G_{2,\mathbf{H}}|$ and $|G_{2,\mathbf{H}}(\Phi)|$, the S_2 function results:

$$\begin{aligned} S_2 &= \sum_{\mathbf{H}} \big(|G_{2,\mathbf{H}}| - \langle |G_2| \rangle\big) |G_{2,-\mathbf{H}}(\Phi)| \\ &= (1/N^{1/2}) \sum_{\mathbf{H}} \big(|E_{\mathbf{H}}| - \langle |E| \rangle\big) |G_{2,-\mathbf{H}}(\Phi)|, \end{aligned} \tag{14}$$

wherein use of equation (10) is made in the second expression. If equation (13) is substituted for $|G_{2,\mathbf{H}}(\Phi)|$ in equation (14), then, in view of equation (7), S_2 becomes

$$\begin{aligned} S_2 = V^{-2} \sum_{\mathbf{H}} D_{\mathbf{H}} \sum_{\mathbf{K}} |M_{\mathbf{K}}| \sum_{\mathbf{h}} |E_{-\mathbf{h}}| |E_{\mathbf{h}-\mathbf{H}-\mathbf{K}}| \\ \times \exp i(\alpha_{\mathbf{K}} + \varphi_{-\mathbf{h}} + \varphi_{\mathbf{h}-\mathbf{H}-\mathbf{K}}) \end{aligned} \tag{15}$$

and, by changing the sum order, it takes the final form

$$S_2 = \sum_{\mathbf{h}} |E_{-\mathbf{h}}| \exp(i\varphi_{-\mathbf{h}}) \Big(V^{-2} \sum_{\mathbf{H}} D_{\mathbf{H}} \sum_{\mathbf{K}} M_{\mathbf{K}} E_{\mathbf{h}-\mathbf{H}-\mathbf{K}} \Big). \tag{16}$$

Expression (16) is the extension of the S function to the more general situation where mixed positive and negative density-function peaks may be present. The quantity between brackets is the Fourier coefficient Q of the product function $\rho_Q = \rho_2' \rho m$ (Fig. 1). For the special case that all scatterers have the same sign, then $m(\mathbf{r}) = 1$ for all $\mathbf{r} \in V$. This implies that $M_{\mathbf{K}}$ will be zero for $\mathbf{K} \neq 0$ and equal to V for $\mathbf{K} = 0$, so that equation (16) reduces to equation (8). Introduction of Q allows equation (16) to be written in the more compact form

$$S_2 = K \sum_{\mathbf{h}} |E_{-\mathbf{h}}| \exp(i\varphi_{-\mathbf{h}})\, Q_{\mathbf{h}}(\Phi). \tag{17}$$

Finally, in parallel to the S function, the new estimates of φ maximizing S_2 can be obtained from

$$\varphi_{\mathbf{h}(\text{new})} = \text{phase of } \big\{ Q_{\mathbf{h}}(\Phi_{\text{old}}) \big\}. \tag{18}$$

All $Q_{\mathbf{H}}(\Phi_{\text{old}})$ and, consequently, all new phase estimates φ, are calculated simultaneously applying the FFT algorithm. Like S-FFT, the S_2-FFT procedure does not involve the condition $\psi_{\mathbf{h}} = \varphi_{\mathbf{h}}$. Hence the refinement will produce either ρ or $-\rho$ as solutions when starting from random phases. The S_2-FFT phase-refinement algorithm used for maximizing the S_2 function is essentially the S-FFT algorithm already published by Rius *et al.* (2007), slightly modified to incorporate the mask in the calculation of ρ_Q. The corresponding flow chart is shown in Fig. 1.

3. Test calculations of the S_2-FFT algorithm

3.1. Comparison with S-FFT

The test calculations were performed on the intensity data of the crystal structures summarized in Table 1 with $t = 2.5$ in equation (11). The finality of these calculations is to check the viability of the above procedure for compounds possessing at least one medium-heavy scatterer in the unit cell. This includes most inorganic and coordination compounds. Inspection of Table 1 clearly indicates that in such cases the number of correct solutions obtained with and without the equal-sign condition is comparable. This result confirms the tolerance of the method to the presence of scatterers with different absolute strength in the unit cell, *i.e.* when the equality (10) is only approximately fulfilled. For structures lacking moderate scatterers, the number of correct solutions with S_2-FFT is smaller than that with S-FFT (*e.g.* Tval in Table 1). This seems to indicate that some improvements in the optimization

Table 1
Application of the S_2-FFT algorithm to single-crystal data.

The results with and without the equal-sign condition are comparable except for Tval, a purely organic compound.

				No. of correct solutions/No. of trials	
Code	Formula	Z	Space group	Without equal-sign condition	With equal-sign condition
Jul1	$C_9H_{10}Cl_3N_3$	8	$P4_12_12$	3/25	3/25
Jul3	$C_{14}H_{22}S_2Si_2$	2	$P2_1/n$	8/25	10/25
Jul4	$C_{11}Cl_{10}$	4	$P2_1/n$	6/25	4/25
Jul5	$C_{11}HCl_9$	4	$Pca2_1$	22/25	25/25
Hov1	$Pr_{14}Ni_6Si_{11}$	4	$C2/m$	21/25	22/25
Bobby	$C_6H_6CaNNaO_6$	4	$P2_13$	9/25	7/25
Cds	$Cd_4SO_{11.5}H_9$	4	$P6_3$	24/25	25/25
Fina13	$C_{14}H_{19}Cl_3N_2O_6Zn$	2	$P1$	25/25	25/25
Cuimid	$C_6H_8ClCuN_4$	6	$P3_221$	6/25	5/25
Tval	$C_{54}H_{90}N_6O_{18}$	2	$P1$	8/121	21/25

The references for the test structures are as follows: Jul1: Julià *et al.* (1992); Jul3: Alemán *et al.* (1993); Jul4 and Jul5: Carilla *et al.* (1995); Hov1: Hovestreydt *et al.* (1983); Bobby: Barnett & Uchtman (1979); Cds: Loüer *et al.* (2001); Fina13: Pons *et al.* (2006); Cuimid: Clegg *et al.* (1984); Tval: Karle (1975) and Smith *et al.* (1975).

Table 2
Application of S_2-FFT to neutron diffraction data.

The success rate is three from 25 trials. All atoms with absolute relative height greater than 90 are listed. Compound data: a = 5.499, b = 7.770, c = 5.542 Å; space group: *Imma*; unit formula: $(Bi_{0.75}Sr_{0.25})MnO_3$, Z = 4.

Atom	Relative height	x/a	y/b	z/c	Site
Bi,Sr	1000	0	1/4	0.9974	4*e*
Mn	−579	1/2	0	0	4*b*
O1	474	1/2	3/4	0.0501	4*e*
O2	409	1/4	0.0275	1/4	8*g*

procedure are still necessary to deal with purely organic compounds.

3.2. Application to neutron diffraction data

The utility of S_2-FFT for finding negative neutron scatterers is checked with the help of two examples. The first example consists of its application to a perovskite-related compound with unit formula $(Bi_{0.75}Sr_{0.25})MnO_3$, which contains the strong negative neutron scatterer Mn (Frontera *et al.*, 2004). The Fermi lengths for Bi, Sr, Mn and O are, respectively, 0.853, 0.702, −0.373 and 0.580. The crystal data are a = 5.499, b = 7.770, c = 5.542 Å, space group *Imma*, Z = 4. The intensities used in the calculations were extracted from the observed powder diffraction pattern by redistributing the global intensities of the overlapped peaks according to the calculated individual intensities. The success rate is three sets from a total of 25. Table 2 contains the peaks in the E map.

The second test example is the application of the S_2-FFT procedure to the single-crystal neutron diffraction data of the 1,3,5-triiodo-2,4,6-trimethylbenzene molecule (Fig. 2). The single-crystal neutron diffraction study of this molecule was published by Boudjada *et al.* (2002). The neutron intensities

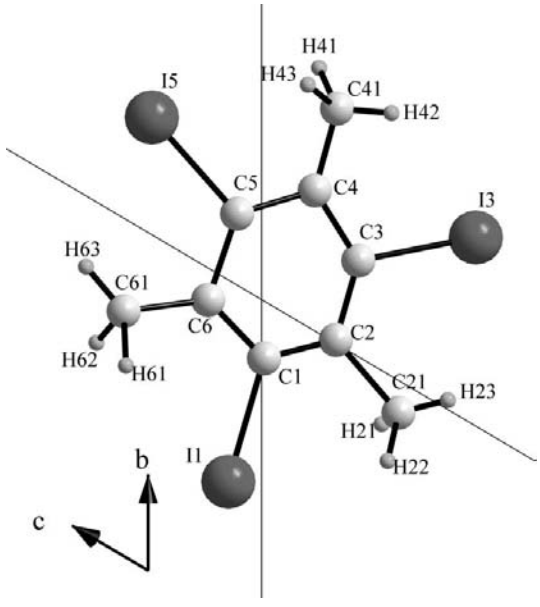

Figure 2
View of the $C_9H_9I_3$ molecule drawn from the peak positions found in the E map after application of S_2-FFT (Table 3).

Table 3
Relative heights and positions of the peaks showing up in the E map after application of S_2-FFT to neutron diffraction data.

Compound data: a = 7.905, b = 9.510, c = 9.521 Å, α = 60.41, β = 66.64, γ = 86.24°; space group: $P\bar{1}$; molecular formula: $C_9H_9I_3$, Z = 2.

Atom	Height	x/a	y/b	z/c
C1	997	0.2443	0.8996	0.9947
C2	992	0.2704	0.0061	0.8369
C3	1000	0.2625	0.1680	0.7876
C4	999	0.2544	0.2457	0.8832
C5	987	0.2468	0.1248	0.0537
C6	969	0.2320	0.9441	0.1174
I1	617	0.2434	0.6473	0.0729
I3	697	0.2813	0.3299	0.5295
I5	722	0.2007	0.2052	0.2409
C21	879	0.2793	0.9436	0.6993
C41	997	0.2576	0.4118	0.8341
C61	924	0.2275	0.8372	0.3029
H21	−380	0.1519	0.9063	0.7365
H22	−408	0.3820	0.8480	0.7231
H23	−347	0.3418	0.0169	0.5906
H41	−340	0.1376	0.4647	0.8736
H43	−334	0.3282	0.4604	0.7147
H43	−219	0.3338	0.4234	0.8984
H61	−415	0.3318	0.7445	0.2977
H62	−385	0.1213	0.7542	0.3623
H63	−185	0.2028	0.8763	0.3854

were collected at 15 K on the D9 four-circle diffractometer at the high-flux reactor of ILL (Grenoble, France). The monochromator was a copper single crystal selecting the 220 reflection, giving λ = 0.70379 Å (crystal data: a = 7.905, b = 9.510, c = 9.521 Å, α = 60.41, β = 66.64, γ = 86.24°, V = 563.7 Å^3; space group: $P\bar{1}$; molecular formula: $C_9H_9I_3$, Z = 2; crystal dimensions: 4 × 2 × 1 mm). Owing to detector problems only 2071 reflections could be measured ($-4 < h < 8$, $-9 < k < 9$, $-9 < l < 9$). Averaging of the equivalent data gave 1079 independent reflections. The Fermi lengths for C, I and H are, respectively, 0.665, 0.528 and −0.374. The parameters defining the direct-methods S_2 phase-refinement function are $\langle|E|\rangle$ = 1.073, d_{min} = 0.82, (No. $|E|_{large}$)/(No. $|E|_{weak}$) = 0.92, strongest $|E|$ value = 3.46, lowest $|E|$ value = 1.35, number of sets 100, maximum number of cycles 39. Phase refinement with S_2-FFT in $P1$ always gives the correct solution (30% for $P\bar{1}$). Table 3 lists the peaks showing up in the E map.

3.3. Application to superstructure reflections

The application of S_2 to the determination of difference structures is illustrated using the superstructure reflections of the double-layer mineral wermlandite (Rius & Allmann, 1984). The crystal structure of wermlandite consists of two alternating layers: a brucite-like layer of composition $[Mg_7(Al_{0.57}Fe_{0.43})_2(OH)_{18}]^{2+}$ and a completely ordered interlayer of composition $[(Ca_{0.6}Mg_{0.4})(SO_4)_2(H_2O)_{12}]^{2-}$. The atomic arrangement of the upper half of the interlayer is shown in Fig. 3(*a*), with the atoms forming the complementary structure (= true structure-substructure) in white (cell dimensions: a = 9.303, c = 22.57 Å; space group: $P\bar{3}c1$; Z = 2). The hkl reflections with l even are much stronger than those with l odd (19 and 47% unobserved reflections, respectively).

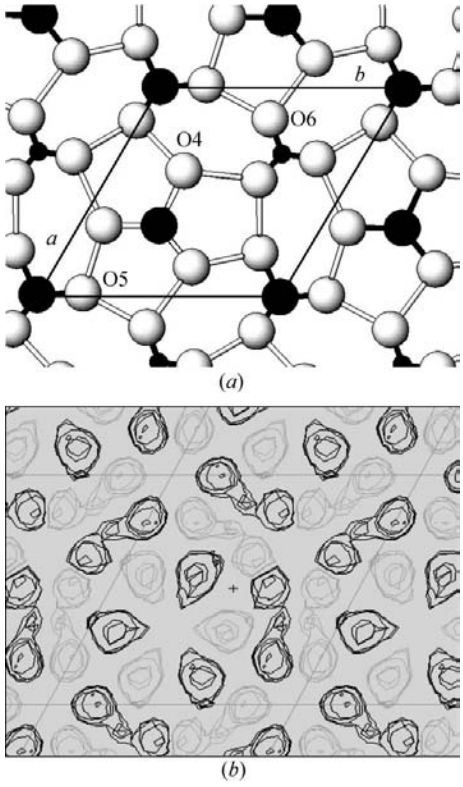

Figure 3
Application of S_2-FFT to difference structures. (*a*) Interlayer of wermlandite. For clarity, only the portion of the interlayer at $z \simeq 0.08$ is presented (with the hydrogen bonds represented by double lines). The rest of the interlayer is related by the inversion center at the origin. Ca^{2+} at (0, 0, 0) is octahedrally coordinated by H_2O5, which is hydrogen bonded to O6 (basis of the SO_4^{2-} group) and H_2O4. Atom O7 (apex of the SO_4^{2-} group) acts as an acceptor of three hydrogen bonds from H_2O4 [S and O7 at (1/3, 2/3, 0.057) and (2/3, 1/3, 0.005), respectively]. Only H_2O4, H_2O5 and O6 have $P\bar{3}c1$ symmetry. (*b*) Section (x, y, $z \simeq 0.08$) of the difference structure δ of wemlandite obtained by applying S_2-FFT to superstructure intensities only (black: positive values; grey: negative values). Notice the nearly exact correspondence between the positive peaks of δ and the positions of H_2O4, H_2O5 and O6 in (*a*). Image obtained with *FAN* (Vernoslova & Lunin, 1993).

The average ($\langle\rho\rangle$) and difference ($\delta = \rho - \langle\rho\rangle$) structures have the same unit cell except for the c parameter, which is doubled for δ ($c = 2c'$). The c' distance corresponds to the separation between the brucite-like main layer and the interlayer. Since the index n of the symmetry reduction is 2, both δ and $-\delta$ are equivalent. According to their symmetry, the atoms in wermlandite can be grouped into the following:

(*a*) Atoms with $P\bar{3}m1$ symmetry, *i.e.* the main layer atoms and Ca, S and the apical O atom of the sulfate group. Since $P\bar{3}m1$ is the symmetry of $\langle\rho\rangle$, they will not contribute to δ and will be ignored.

(*b*) Atoms with $P\bar{3}c1$ symmetry, *i.e.* the water molecules O4 and O5, and O6, the O atom of the basis of the sulfate group. Since the superstructure is of index 2, the corresponding averaged positions in $\langle\rho\rangle$ have half-weight. The peaks in δ will appear as separate positive and negative peaks with half-weight.

Fig. 3(*b*) reproduces the electron-density distribution obtained from the application of S_2-FFT to the superstructure reflections (27 strong and 22 weak reflections, $\langle|E|\rangle = 1.01$, 7% successful runs). The positive and negative maxima of δ can be clearly seen. From these peaks it is immediate to derive the complementary structure.

This work was supported by the Spanish 'Ministerio de Eduación y Ciencia' (projects MAT2005-01736 and CSD 2007-00041) and by the 'Generalitat de Catalunya' (SGR2005-00452). The authors express their gratitude to Dr M. Teresa Fernández-Diaz at ILL for kindly supplying the single-crystal neutron diffraction data.

References

Alemán, C., Brillas, E., Davies, A. G., Fajarí, L. L., Giró, D., Julià, L., Pérez, J. J. & Rius, J. (1993). *J. Org. Chem.* **58**, 3091–3099.
Barnett, B. L. & Uchtman, V. A. (1979). *Inorg. Chem.* **18**, 2674–2678.
Boudjada, A., Meinnel, J. J., Boucekkine, A., Hernandez, O. J. & Fernández-Diaz, M. T. (2002). *J. Chem. Phys.* **117**, 10173–10183.
Carilla, J., Fajarí, Ll., García, R., Julià, L., Marcos, C., Riera, J., Whitaker, C. R., Rius, J. & Alemán, C. (1995). *J. Org. Chem.* **60**, 2721–2725.
Clegg, W., Acott, S. R. & Garner, C. D. (1984). *J. Chem. Soc. Dalton Trans.* pp. 2581–2584.
Cochran, W. (1955). *Acta Cryst.* **8**, 473–478.
Debaerdemaeker, T. de & Woolfson, M. M. (1983). *Acta Cryst.* A**39**, 193–196.
DeTitta, G. T., Weeks, C. M., Thuman, P., Miller, R. & Hauptman, H. A. (1994). *Acta Cryst.* A**50**, 203–210.
Frontera, C., García-Muñoz, J. L., Aranda, M. A. G., Hervieu, M., Ritter, C., Mañosa, L., Capdevila, X. G. & Calleja, A. (2004). *Phys. Rev. B*, **68**, 134408.
Germain, G., Main, P. & Woolfson, M. M. (1970). *Acta Cryst.* B**26**, 274–285.
Hirnet, A., Schroeder, K., Blügel, S., Torrelles, X., Albrecht, M., Jenichen, B., Gierer, M. & Moritz, W. (2002). *Phys. Rev. Lett.* **88**, 226102.
Hovestreydt, E., Klepp, K. & Parthé, E. (1983). *Acta Cryst.* C**39**, 422–425.
Julià, L., Rius, J. & Suschitzky, H. (1992). *Heterocycles*, **34**, 1539–1545.
Karle, I. L. (1975). *J. Am. Chem. Soc.* **97**, 4379–4386.
Karle, J. & Hauptman, H. (1956). *Acta Cryst.* **9**, 635–651.
Loüer, D., Rius, J., Bènard-Rocherullé, M. & Loüer, M. (2001). *Powder Diffr.* **16**, 86–91.
Pons, F., Rius, J. & Ros, J. (2006). *Inorg. Chim. Acta*, **359**, 379–382.
Rius, J. (1993). *Acta Cryst.* A**49**, 406–409.
Rius, J. (2006). *Acta Cryst.* A**62**, 331–335.
Rius, J. & Allmann, R. (1984). *Z. Kristallogr.* **168**, 133–134.
Rius, J., Crespi, A. & Torrelles, X. (2007). *Acta Cryst.* A**63**, 131–134.
Rius, J., Miravitlles, C. & Allmann, R. (1996). *Acta Cryst.* A**52**, 634–639.
Smith, G. D., Duax, W. L., Langs, D. A., DeTitta, G. T., Edmonds, J. W., Rohrer, D. C. & Weeks, C. M. (1975). *J. Am. Chem. Soc.* **97**, 7242–7247.
Torrelles, X., Rius, J., Boscherini, F., Heun, S., Mueller, B. H., Ferrer, S. & Alvarez, J. (1998). *Phys. Rev. B*, **57**, R4281.
Vernoslova, E. A. & Lunin, V. Yu. (1993). *J. Appl. Cryst.* **26**, 291–294.